Physico Chemical Principles of CEST

Robert E. Lenkinski, PhD

Department of Radiology, Beth Israel Deaconess Medical Center

Boston MA, USA

rlenkins@bidmc.harvard.edu

We have recently reviewed the principles and applications of chemical exchange saturation transfer (CEST) in MR (1).

A Simple Model of the CEST Effect**.** The simplest model for CEST, is the two pool model which although is too simplistic to explain all of the interactions present *in vivo*, forms the conceptual for mathematical descriptions of the CEST effect. In this model (shown in Figure 1) there are two pools of spins --agent-bound protons (pool A) and free or bulk water protons (pool B).

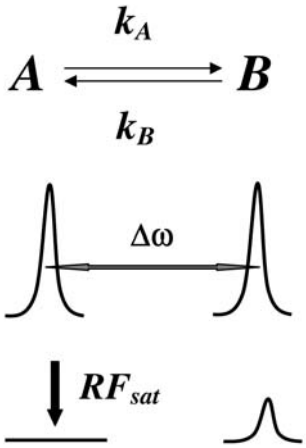

Figure 1: Schematic depiction of chemical exchange between two pools of proton spins A and B. The lower part of the graph shows a decrease in pool B signal following selective RF saturation of pool A.

In the simplest CEST experiment one applies a frequency-selective RF irradiation to the agent-bound spins until all of the nuclear magnetizations reach a steady state and then samples the remaining longitudinal magnetization of the bulk water protons. Ideally, the selective RF irradiation pulse does not directly affect the bulk water protons. The maximum CEST effect occurs when the RF completely saturates the agent-bound protons so that their longitudinal magnetization is zero. Chemical exchange causes transfer of protons from pool A at a transition rate of k_A that is by definition $1/\tau_A$ (τ_A, lifetime of a proton in pool A). In this case, a proton that leaves pool B, characterized by transition rate k_B (= $1/\tau_B$), is replaced via chemical exchange with a proton that has zero Z magnetization.

This exchange causes the Z-magnetization to decrease at the rate of $k_B M_Z^B$ (M_Z^B = Z magnetization in pool B) and results in a drain of magnetization from pool B, whose equilibrium Z magnetization is M_0^B. At the same time, the inherent spin–lattice relaxation

of pool B (i.e. $[M_0^B - M_Z^B]/T_{1B}$) tends to increase the Z magnetization back towards the equilibrium value. The net rate of change of Z magnetization (dM_Z^B/dt) is the difference between these two rates. M_Z^B decreases until a steady state value is reached, M_Z^B (ss), where these two rates are equal according to Eq 1; rearrangement of Eq 1 to Eq 2 gives the Z value. By dividing both the numerator and the denominator of Eq. 2 by τ_B, and using the detailed balance equation $c_B/\tau_B = c_A/\tau_A$ (with c_A=concentration of protons in pool A, c_B=concentration of protons in pool B, usually 111 Molar), one obtains Eq 3

$$k_B M_Z^B(ss) = \frac{\left(M_0^B - M_Z^B(ss)\right)}{T_{1B}} \qquad [1]$$

$$Z = \frac{M_z^B(ss)}{M_0^B} = \frac{\tau_B}{T_{1B} + \tau_B} \qquad [2]$$

or

$$Z = \frac{1}{1 + \frac{T_{1B}}{\tau_B}} = \frac{1}{1 + \frac{c \cdot n}{111}\frac{T_{1B}}{\tau_A}} \qquad [3]$$

where the symbols are defined as: k_B, the exchange rate of protons in pool B (1/s); M_Z^B(ss), the longitudinal magnetization of pool B at steady state; T_{1B}, the longitudinal relaxation time of pool B (s); τ_B, the lifetime of protons in pool B (s); c, the molar concentration of the CEST agent (moles/L); *n*, the number of exchanging protons per CEST molecule; and τ_A, the lifetime of protons in pool A (s).

Equation 3 predicts how some of the properties of the CEST agent alter the observed CEST effect; the longer the longitudinal relaxation time of the bulk water, the stronger the CEST effect. This means that higher magnetic fields, with their associated longer longitudinal relaxation times yield larger CEST effects. Additionally, the maximum CEST effect is obtained when τ_A is short.

Equation 3 also predicts the detection limit of a CEST agent with known bound water lifetime in an environment (bulk water) characterized by a given T_{1B}. For example, for an agent with τ_A of 3 μs, T_{1B} of 1 s, and 2 exchanging protons per CEST molecule, assuming a frequency-selective pre-saturation sequence can be implemented to fully saturate the bound water, Eq 3 predicts that the bulk water signal intensity can be reduced by about 37% with 100 μM agent, and 5% with 10 μM agent.

The latter concentration is well below the detection limit expected for a low molecular weight Gd^{3+} based contrast agent with a typical relaxivity of 4–5 $mM^{-1}s^{-1}$ (2). These data suggest that CEST agents have the potential to be more sensitive than Gd^{3+} based T_1 agents, assuming that all of the practical aspects of imaging these agents, such as complete saturation of pool A, can be achieved. Just as one can increase the relaxivity of Gd^{3+} based agents substantially by conjugation to a polymer or formation of an aggregate (3-5), similar modifications of paramagnetic CEST agents may be envisioned. Such modifications would easily extend the lower detection limit into the sub-μM range

and may prove useful for imaging targets that are present at relatively low concentrations. A series of polymers containing large numbers of exchangeable –NH groups have already been described for this purpose (6).

Although the above basic description provides some useful insight into the potential sensitivity of CEST agents, it is based on a few unrealistic assumptions. First, it assumes that saturation of the bound protons does not directly affect the bulk water signal. This assumption may not be valid, in particular for DIACEST agents in which the exchangeable proton resonances lie relatively close to the water signal. Second, it assumes that the agent protons can be fully saturated by RF irradiation. This is also unlikely to be fully satisfied in a clinical scanner, especially for PARACEST agents, for two main reasons.

1. Clinical coils usually have a limited capability of providing saturation (or B_1) fields larger than a given value (25 μT is typical). Although imaging DIACEST agents is amenable to lower presaturation fields, rapidly exchanging PARACEST agents may require stronger fields. RF amplifiers also have a limited capability of providing continuous RF amplification exceeding a duration of 20–60 ms. It is, therefore, technically difficult to provide constant amplification (with no drop-off) at high presaturation powers.

2. Continuous or semi-continuous RF irradiation of the patient may exceed the guidelines set by the Food and Drug Administration (FDA) for the amounts of RF power that can be deposited in a human subject. This is usually referred to as specific absorption rate, or SAR, which is a complex function of RF coil design, patient weight, the particular imaging sequence employed, and the anatomical region under study. For human whole body imaging, e.g., FDA limits SAR to 4W/kg for any 15-minute period.

Multi-pool Models of the CEST Effect. A more complete model of the CEST effect takes into account 1) direct water saturation, and 2) potentially incomplete saturation of pool A protons. In the simplest scenario, only two pools of protons can be considered (7). It is common, however, that a three-pool model is used to explain the dynamics of the system. In particular, PARACEST agents often have a lanthanide-bound water (pool A), a bulk water (pool B), and the –NH protons of the rare earth chelate (pool C) (7). Fig. 2 depicts the typical couplings between these three proton pools in which the two exchanging pools of the CEST agent are assumed to exchange protons only with the free water pool, but not with each other.

Figure 2: Typical coupling between two pools of exchangeable protons in PARACEST agents, pool A and pool C. An approximation is usually made that they only exchange protons with the bulk water pool (pool B), but not between each other.

In such a 3-pool system, the dynamics of the magnetization vectors is described by nine Bloch equations modified for chemical exchange (7, 8). Even this 3-pool model is only a mathematical approximation of the situation encountered *in vivo*. While sometimes

a 2-pool model might suffice for explaining the measured CEST signal, more complicated situations than the ones described by a 3-pool model can also arise. In addition to free water molecules, living tissues contain water molecules bound to proteins, exchangeable protein protons, and so forth. In such cases, a model with four or more pools might be needed to describe the magnetization dynamics *in vivo* (9, 10).

Although extending the 3-pool model further adds refinements and may provide slightly better fits to data acquired *in vivo*, it also adds complexity. For example, a 4-pool model is composed of 12-coupled differential equations. Not only does such a system of equations become more difficult to solve, but it also has a large number of variables; it has 14 unknowns—8 relaxation rates (2 for each pool), 3 proton lifetimes and 3 concentrations. Additionally, four chemical shifts exist for the 4 species that may be treated as constant or variable (chemical shits may change due to environmental parameters or B_0 inhomogeneities, e.g.). Since only a limited number of data points can be acquired *in vivo*, data fitting using such a model may become unstable and result in uncertain measurements. A chemical system whose dynamics may require more than 3 pools to describe has been described by Li et al. (9).

Experimentally in an NMR or *in vitro* study, the CEST effect is typically measured from a plot of residual bulk water proton Z magnetization versus the frequency offset of the saturation pulse, varied over a range of frequencies that include the Larmor frequencies of both proton pools. The resulting plot is referred to as a Z spectrum (11) or CEST spectrum (12). Fig. 3 displays the Z spectra collected at 7 T on a 50 mM aqueous solution of Europium (III) [1,4,7,10-tetraazacyclododecane-1,4,7,10-tetra(ethyl-acetamidoacetate), a typical Eu^{3+}DOTA-tetraamide complex. The points are the measured Z data at field (B_1) values of 110, 160, 230, 320 and 450 Hz (in descending order in the graph). The solid lines are fits of the experimental data using the Bloch equations for a 3-pool model, namely Eu^{3+}-bound water, bulk water, and amide NH (NB: the CEST effect increases with increasing saturation field).

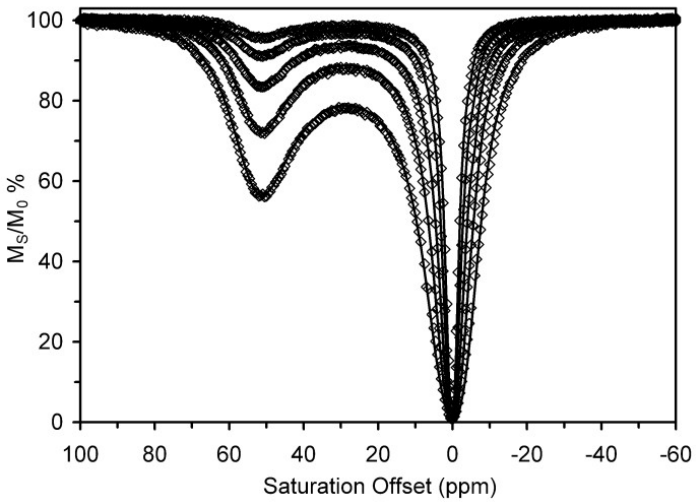

Figure 3: Z spectra recorded at 7 T for a 50-mM aqueous solution of (Eu(3)-DOTA-tetraamide). The points are the measured Z data at field (B_1) values of 110, 160, 230, 320 and 450 Hz (in descending order in the graph). The solid lines are fits of the experimental data using Bloch equations for a 3-pool model (Eu^{3+}-bound water, bulk water, and amide NH).

The Determination of CEST Proton Lifetimes of Exchange. It is possible to characterize a given CEST agent and, in particular, to determine its chemical shift(s) and exchange rate(s) by fitting a Z spectrum with a large number of data acquired *in vitro*. The assumption made in this approach, however, becomes questionable *in vivo*. The imaging time must be minimized for patient comfort and economic reasons. It is also essential to limit the SAR delivered to the patient (due to RF power deposition during agent saturation). These factors limit the number of data points that can be acquired *in vivo*. Consequently, once a given agent is characterized *in vitro* and its approximate chemical shift(s) are determined, irradiation is performed *in vivo* at a minimal number of frequencies (13).

Usually the agent is irradiated at its resonant frequency and at a frequency situated symmetrically opposite to it in the Z spectrum (the negative of the resonance frequency with respect to the water peak). The measure of signal enhancement due to the CEST agent is usually presented as %Contrast, according to Eq 4. This definition takes into consideration the direct saturation of the water signal by the saturation pulse which may be significant for certain types of CEST agents in particular diamagnetic agents.

$$\%\text{Contrast} = \frac{S(-\omega_{res}) - S(\omega_{res})}{S(-\omega_{res})} \qquad [4]$$

where $S(\omega_{res})$ is the signal at resonance frequency of the CEST agent; and $S(-\omega_{res})$ is the signal at minus resonance frequency of the CEST agent (defined with respect to the water resonance set at 0).

Irradiation at two different frequencies is sufficient to highlight the contrast *in vivo*, but information about proton lifetimes is lost in this way. The measurement of proton lifetime is one of the advantages of CEST agents, allowing quantitative assessment of environmental parameters, such as pH, temperature and metabolite concentrations. The lost information may, however, be recovered even without the Z spectrum by using a small number of irradiation power levels or durations (14). In fact, irradiation with a number of power levels, while keeping RF saturation time at a constant fraction of the repetition time, produces the data for the computation of proton lifetime according to Eq 5; namely, a straight line fit of the inverse CEST effect data against $1/w_1^2$ results in an x-intercept that is equal to $-\tau_A^2$. The complete derivation of this approach is provided in (15)

$$\text{Inverse CEST effect} = \frac{S(\omega_{res})}{S(-\omega_{res}) - S(\omega_{res})} = \alpha(\tau_A + \frac{1}{\omega_1^2 \tau_A}) \qquad [5]$$

where $S(\omega_{res})$ and $S(-\omega_{res})$ are defined as in Eq 4; α is a constant depending on agent concentration, relaxation times, etc, but not on proton lifetime; τ_A is the lifetime of protons in pool A (s); and ω_1 is the strength of RF saturation field (rad/s).

Fig. 4 illustrates an example of this method as plots of inverse CEST effect against $1/\omega_1^2$ for two solutions with concentrations of 20 mM and 60 mM of Europium(III)

[1,4,7,10-tetraazacyclododecane-1,4,7,10-tetra(acetamidoacetic acid)][Eu(DOTAM-Gly)] irradiated with multiple power levels (discrete data points on the graph), providing identical intercepts after straight line fits (15) .

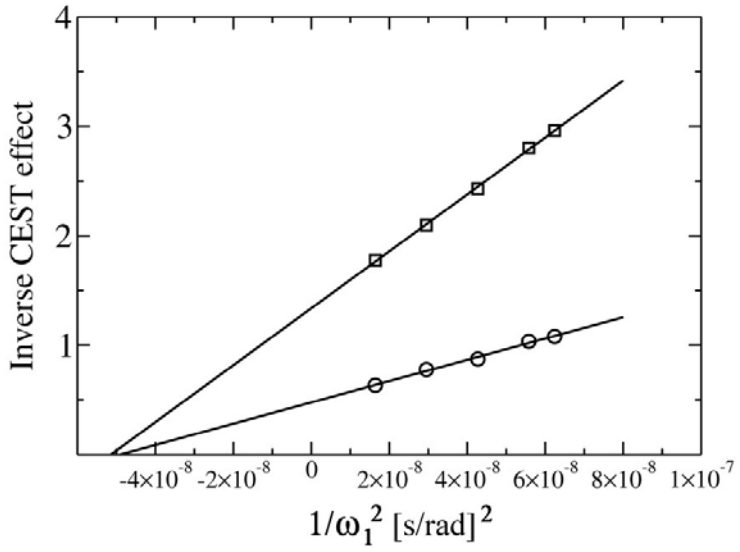

Figure 4: Plots of inverse CEST effect as a function $1/\omega_1^2$ according to Eq 5 for a phantom containing 20 mM (□) or 60 mM (○) of Eu-DOTAM-Gly. The linear fits indicate a common intercept equal to $-\tau_A^2$. For a definition of the symbols see Eq 5.

The proton lifetimes extracted from these x-intercepts are consistent with proton lifetimes extracted from fits of Z spectra of the same two CEST agent solutions. This method enables quantitative extraction of environmental parameters with just 4–6 data sets by irradiating at the agent resonance frequency and symmetrically opposite to the water resonance at 2–3 different power levels. This compares to the 20–40 data sets needed to extract the same information from a Z spectrum.

Agent Design and Saturation Power in CEST Imaging. Equation 3 indicates that the maximum contrast per CEST agent dose is obtained with an agent with the shortest proton lifetime. However, this statement is only correct if the exchanging protons of the CEST agent are fully saturated. If complete saturation of the rapidly exchanging site is not achieved, e.g. due to limitations in B_1 strength or duration imposed by FDA guidelines on SAR, the observed CEST effect would be correspondingly reduced. More complete saturation may then be achieved by slowing the exchange rate, affording more time for saturation to occur. Since these two effects run counter to one another, a value of τ_A which maximizes the CEST effect for a given B_1, i.e. τ_{A_Max}, can be found from Eq. 6 (7).

$$\tau_{A\_Max} = 1/(2\pi B_1) = 1/\omega_1 \qquad [6]$$

where τ_{A_Max} is the value of proton lifetime in pool A that maximizes the CEST signal for a given allowable B_1 (s); B_1 is the strength of RF saturation field (Hz); and ω_1 is the strength of RF saturation field (rad/s)

Fig. 5 illustrates the simulation of the CEST effect (defined as % contrast) as a function of applied B_1.

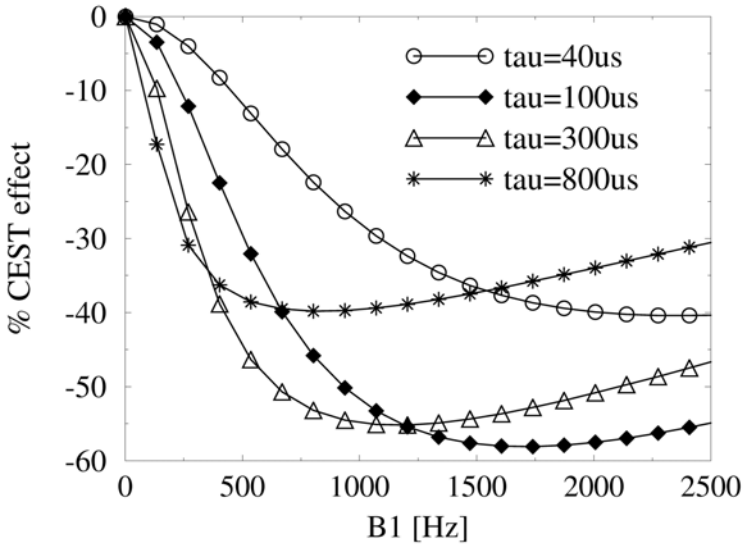

Figure 5: Theoretical simulation of % contrast for a CEST agent as a function of RF strength for various proton exchange lifetimes. Simulations were performed using a 3-pool Bloch model, as described in the text.

This simulation includes the saturation pulse applied during ~50% of the repetition time for four hypothetical PARACEST agents having identical characteristics, except for their τ_A which varies between 40 and 800 μs. The simulation was performed with a 3-pool model, with pool A concentration of 62.5 mM shifted by 50 ppm and pool C containing 130 mM of exchangeable protons shifted by 6 ppm with lifetime τ_A = 8 ms and with bulk water lifetimes of T_{1B} = 2.8 s and T_{2B} = 1.7 s.

If a B_1 of about 300 Hz is allowed at 50% duty cycle, which is close to the maximum admissible for a 1.5 T head scan, the agent with the maximum contrast must have a τ_A of about 500 μs. An allowable B_1 of 1000 Hz, which is potentially permissible when imaging smaller field of view with a smaller coil, would favor a PARACEST agent with τ_A of about 100 μs.

However, with very high B_1 values and low chemical shifts, the control irradiation tends to decrease image intensity and thus reduce the observed % contrast. This will limit the CEST effect at high B_1, as evident by tilting of the curves in Fig. 5.

References

1. Hancu I, Dixon WT, Woods M, Vinogradov E, Sherry AD, Lenkinski RE. CEST and PARACEST MR contrast agents. Acta Radiologica. 2010 Oct;51(8):910-23.
2. Ahrens ET, Rothbacher U, Jacobs RE, Fraser SE. A model for MRI contrast enhancement using T1 agents. PNAS. 1998;95(15):8443-8.
3. Lauffer RB, Betteridge DR, Padmanabhan S, Brady TJ. Albumin binding of paramagnetic hepatobiliary contrast agents: enhancement of outer sphere relaxivity. Nucl Med Biol. 1988;15(1):45-6.
4. Toth E, Van Uffelen I, Helm L, Merbach AE, Ladd D, Briley-Saebo K, Kellar KE. Gadolinium-based linear polymer with temperature-independent proton relaxivities: a unique interplay between the water exchange and rotational contributions. Magn Reson Chem. 1998;36(Spec. Issue):S125-S34.
5. Bogdanov A, Matuszewski L, Bremer C, Petrovsky A, Weissleder R. Oligomerization of Paramagnetic Substrates Results in Signal Amplification and Can Be Used for MR Imaging of Molecular Targets. *Molecular Imaging*. 2001;1:1 - 9.
6. Goffeney N, Bulte JW, Duyn J, Bryant LH, Jr., van Zijl PC. Sensitive NMR detection of cationic-polymer-based gene delivery systems using saturation transfer via proton exchange. J Am Chem Soc. 2001 Sep 5;123(35):8628-9.
7. Woessner DE, Zhang S, Merritt ME, Sherry AD. Numerical solution of the bloch equations provides insights into the optimum design of PARACEST agents for MRI. Magn Reson Med. 2005;53(4):790-9.
8. Baguet E, Roby C. Off-resonance irradiation effect in steady-state NMR saturation transfer. J Magn Reson. 1997 Oct;128(2):149-60.
9. Li AX, Hudson RH, Barett J, Bartha R, editors. Four-pool modeling of proton exchange in biological systems in the presence of MRI-PARACEST agents. Proc Intl Soc Magn Reson Med; 2008; Toronto.
10. Li AX, Hudson RHE, Barrett JW, Jones CK, Pasternak SH, Bartha R. Four-Pool Modeling of Proton Exchange Processes in Biological Systems in the Presence of MRI-Paramagnetic Chemical Exchange Saturation Transfer (PARACEST) Agents. Magnetic Resonance in Medicine. 2008 Nov;60(5):1197-206.
11. Grad J, Bryant RG. Nuclear magnetic cross-relaxation spectroscopy. J Magn Reson. 1990;90:1 - 8.
12. Ward KM, Aletras AH, Balaban RS. A New Class of Contrast Agents for MRI Based on Proton Chemical Exchange Dependent Saturation Transfer (CEST). J Magn Reson. 2000;143(1):79-87.
13. Sun PZ, Zhou J, Huang J, van Zijl P. Simplified quantitative description of amide proton transfer (APT) imaging during acute ischemia. Magn Reson Med. 2007 Feb;57(2):405-10.
14. McMahon MT, Gilad AA, Zhou J, Sun PZ, Bulte JW, van Zijl PC. Quantifying exchange rates in chemical exchange saturation transfer agents using the saturation time and saturation power dependencies of the magnetization transfer effect on the magnetic resonance imaging signal (QUEST and QUESP): Ph calibration for poly-L-lysine and a starburst dendrimer. Magn Reson Med. 2006 Apr;55(4):836-47.
15. Dixon WT, Ren JM, Lubag AJM, Ratnakar J, Vinogradov E, Hancu I, Lenkinski RE, Sherry AD. A Concentration-Independent Method to Measure Exchange Rates in PARACEST Agents. Magnetic Resonance in Medicine. 2010 Mar;63(3):625-32.